Medical Engineering and Physics 69 (2019) 92–99

Contents lists available at ScienceDirect

Medical Engineering and Physics

journal homepage: www.elsevier.com/locate/medengphy

Design of a novel procedure for the optimization of the mechanical performances of 3D printed scaffolds for bone tissue engineering combining CAD, Taguchi method and FEA

Gregorio Marchiori[a,*], Matteo Berni[b,c], Marco Boi[a], Mauro Petretta[d,g], Brunella Grigolo[d], Devis Bellucci[e], Valeria Cannillo[e], Chiara Garavelli[f], Michele Bianchi[a]

[a] IRCCS Istituto Ortopedico Rizzoli, Laboratorio di NanoBiotecnologie (NaBi), Via di Barbiano 10/2, 40136 Bologna, Italy
[b] IRCCS Istituto Ortopedico Rizzoli, Laboratorio di Biomeccanica e Innovazione Tecnologica, Via di Barbiano 10/2, 40136 Bologna, Italy
[c] Department of Information Engineering, University of Brescia, Via Branze 38, 25123 Brescia, Italy
[d] IRCCS Istituto Ortopedico Rizzoli, Laboratorio RAMSES, Via di Barbiano 10/2, 40136 Bologna, Italy
[e] Dipartimento di Ingegneria Enzo Ferrari, Unità di Ricerca del Consorzio Interuniversitario Nazionale per la Scienza e Tecnologia dei Materiali (INSTM), Università degli Studi di Modena e Reggio Emilia, Via P. Vivarelli 10, 41125 Modena, Italy
[f] Università di Bologna, DEI, Via Zamboni, 33, 40126 Bologna, Italy
[g] RegenHu Ltd., Z.I. du vivier 22, CH-1690, Villaz St. Pierre, Switzerland

ARTICLE INFO

Article history:
Received 22 February 2018
Revised 11 March 2019
Accepted 28 April 2019

Keywords:
Scaffold
Design of experiments
3D printing
Compressive modulus

ABSTRACT

In order to increase manufacturing and experimental efficiency, a certain degree of control over design performances before realization phase is recommended. In this context, this paper presents an integrated procedure to design 3D scaffolds for bone tissue engineering. The procedure required a combination of Computer Aided Design (CAD), Finite Element Analysis (FEA), and Design methodologies Of Experiments (DOE), firstly to understand the influence of the design parameters, and then to control them.

Based on inputs from the literature and limitations imposed by the chosen manufacturing process (Precision Extrusion Deposition), 36 scaffold architectures have been drawn. The porosity of each scaffold has been calculated with CAD. Thereafter, a generic scaffold material was considered and its variable parameters were combined with the geometrical ones according to the Taguchi method, i.e. a DOE method. The compressive response of those principal combinations was simulated by FEA, and the influence of each design parameter on the scaffold compressive behaviour was clarified. Finally, a regression model was obtained correlating the scaffold's mechanical performances to its geometrical and material parameters. This model has been applied to a novel composite material made of polycaprolactone and innovative bioactive glass. By setting specific porosity (50%) and stiffness (0.05 GPa) suitable for trabecular bone substitutes, the model selected 4 of the 36 initial scaffold architectures. Only these 4 more promising geometries will be realized and physically tested for advanced indications on compressive strength and biocompatibility.

1. Introduction

In bone tissue engineering, 3D printed scaffolds are of particular interest for the regeneration of critical bone defects, thanks to the possibility to properly tailor their geometrical features by simply modifying the printing parameters [1,2].

In addition to suitable biocompatibility and osteoconductivity, scaffolds must fulfil strict criteria in terms of mechanical requirements and processability [1]. As is well-known, these criteria are strongly dependent on scaffold design. In particular, scaffold osseointegration has been strictly correlated to its porosity and pore dimension [3–5], whereas the structural integrity of the construct has been closely associated to the compressive response [3,6].

In the attempt to optimize *ab initio* the mechanical performance of 3D porous scaffolds, Computer Aided Design (CAD), Finite Element Analysis (FEA) and Taguchi method (a Design Of Experiments, DOE method) have been investigated as promising

Abbreviations: CAD, Computer Aided Design; FEA, Finite Element Analysis; DOE, Design Of Experiments; PED, Precision Extrusion Deposition; PCL, Polycaprolactone; FIBRE, scaffold fibre diameter; PORE, scaffold pore size; STEP, orientation between successive scaffold fibre planes; OFFSET, offset between scaffold planes with the same fibre orientation; CM, scaffold compressive modulus; SIZE, average finite element dimension of the scaffold mesh.

* Corresponding author.
E-mail address: gregorio.marchiori@ior.it (G. Marchiori).

https://doi.org/10.1016/j.medengphy.2019.04.009
1350-4533/

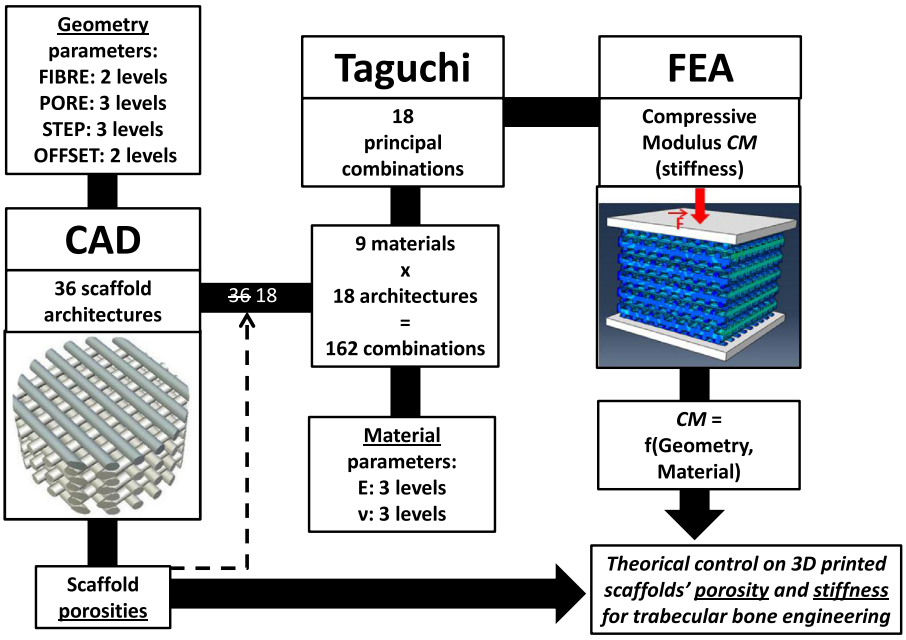

Fig. 1. Scaffold design procedure combining Computer Aided Design (CAD), Taguchi method and Finite Element Analysis (FEA).

solutions. FEA, with or without CAD, had been already exploited in the optimization of both scaffolds architecture [7,8] and composition [9,10]. The Taguchi method is commonly applied to the design of experiments, where the effect of many project parameters on the output of interest is researched, allowing to achieve the best solution by acting only on a very small subset of all the possible parameters combinations; the efficacy of this method at a modelling level - preceding the experimental phase - has already been demonstrated [11]. However, in the case of scaffolds for bone tissue engineering, the use of the Taguchi method had so far been restricted solely to the optimization of manufacturing [12,13] and not to the design of the scaffold prior to fabrication.

Here an innovative procedure is presented, combining for the first time CAD, FEA and the Taguchi method with the specific aim of concurrently controlling scaffold architecture and composition. Thus, to achieve a high level of control over the performances of the construct before its realization, limiting the fabrication step to only the more promising scaffolds.

To demonstrate the efficacy of the proposed procedure, the design was applied to 3D printed scaffolds realized by Precision Extrusion Deposition (PED). As scaffold material, polycaprolactone (PCL) combined with an innovative bioactive glass [14] was selected, since polymeric matrixes embedded with an inorganic phase are of increasing interest in the field of bone tissue engineering, due to the possibility of tailoring the mechanical properties of the scaffold as well as its bioactivity by mixing the proper amount of the components [15].

2. Materials and methods

2.1. Simulation

A scheme of the proposed procedure for the optimization of scaffold design is illustrated in Fig. 1. CAD is used to draw scaffold architectures and calculate their porosities, and then select the geometries to be analysed; the Taguchi method is applied to select the principal combinations of scaffold architecture and generic material; FEA simulates the mechanical performances of those combinations, and the results serve to build up a regression model that controls the effect of any combination of architecture and material on the scaffold design mechanics.

Scaffold architectures have been defined based on the geometric parameters described in literature and adjustable via the manufacturing technique (3D printing) selected in this study: fibre diameter (FIBRE), pore size (PORE), orientation between successive fibre planes (STEP) and offset between planes with the same fibre orientation (OFFSET) (Fig. 2).

Specifically, 3D printing was applied in the form of Precision Extrusion Deposition (PED), in which a material is fed into and extruded by a nozzle that forms the construct, layer by layer. At each deposited layer of the manufacturing process, the printer nozzle moves up by 80% of the diameter of the fibre. In the CAD drawing, this is reflected in an interpenetration between subsequent fibre planes of about 20%. Geometry parameters were changed following a practical approach, i.e. with values achievable by the 3D printer and in any case common in similar applications (e.g. for PORE see Karageourgiou, Kaplan, 2005 [16]): FIBRE 330–840 µm, PORE 300-450-600 µm, STEP 45-60-90°, OFFSET YES/NO. Combining the above parameters resulted in 36 different scaffold architectures. These 36 architectures were drawn through CAD software as cylinders ($\Phi = 10$ mm, $h = 6$ mm) with the following aims: (1) to calculate their porosity, by relating solid and free volume, and (2) to predispose them for the following mechanical simulations.

Scaffold porosity was defined as:

$$Porosity = \left(1 - \frac{V_{sca}}{V_{cyl}}\right) \times 100\ (\%) \tag{1}$$

where V_{sca} is the volume of the CAD scaffold and V_{cyl} is the total volume of the boundary cylinder [6].

In order to control the scaffold porosity by tuning a single parameter, the expression found in [17] is used:

$$Porosity = \frac{a}{1 + (PORE : FIBRE)^c}\ (\%) \tag{2}$$

where PORE:FIBRE is the control parameter, i.e. the ratio between pore size (PORE) and fibre diameter (FIBRE), while a and c are fitting constants. By fixing the desired porosity in Eq. (2), it is possible to know the PORE:FIBRE needed to obtain it. Specifically in the

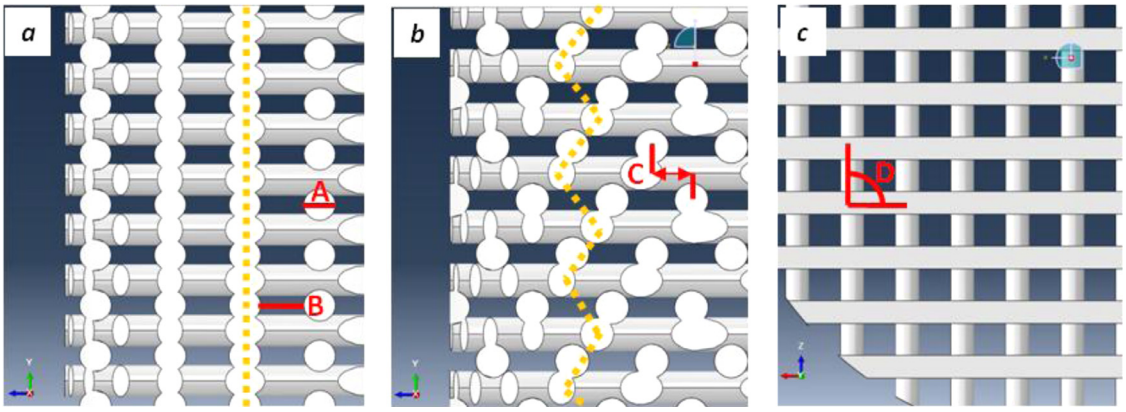

Fig. 2. Partial lateral view (a and b) and partial view from above (c) of CAD scaffolds. Geometrical parameters: A is the fibre diameter (FIBRE), B is the pore size (PORE), C is the OFFSET and D is the STEP. Orange dotted lines indicate vertical (y direction) pillars.

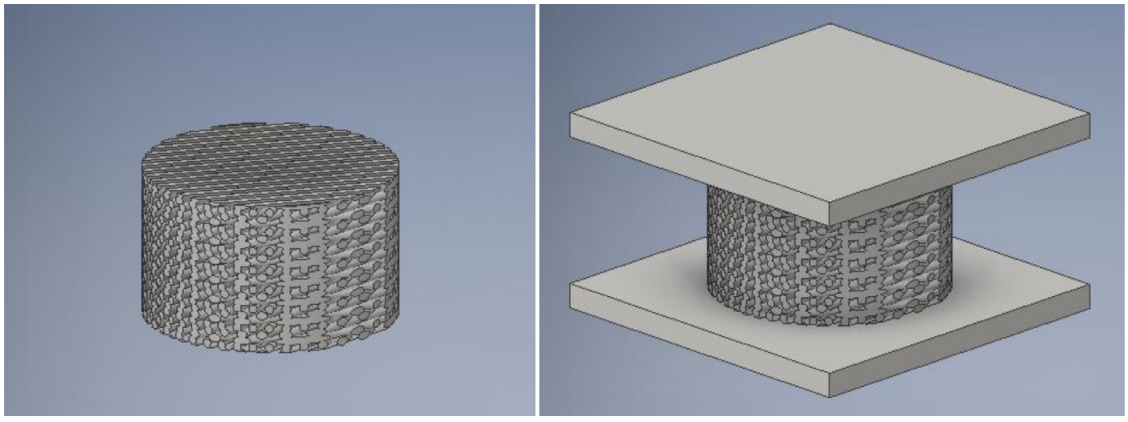

Fig. 3. CAD drawing of a scaffold before (left) and after (right) the application of compressive plates.

case of PED, setting FIBRE (the printer nozzle) allows to know the minimum PORE that needs to be set to the scaffold.

Finally, the realized CAD drawings were prepared for the mechanical simulation. Specifically, compression plates have been added to every cylindrical scaffold, on both the top and bottom surfaces, to simulate the chosen mechanical test (Fig. 3), i.e. axial compression.

Only a subset of the 36 CAD scaffolds, selected by the Taguchi method, underwent mechanical simulation. The Taguchi method is a design of experiments (DOE) method [18], used for investigating the entire range of the input parameters evaluating only a subset of their combinations–i.e. the main ones - which usually results in a remarkable saving of both time and cost, while in this particular case it is constrained to solely time saving as it is limited to the FEA simulations, and not yet the physical experiments.

First of all, the levels of the parameters combined by the Taguchi method - and used as input for FEA on scaffold mechanics–had to be defined. The previous CAD phase established the geometrical parameters. The other FEA input parameters were inherent to the scaffold material and mesh (the body discretization which the FE method is based on). In order to define them, the FEA output must be considered: FEA simulations sought to identify the scaffold compressive modulus (CM), which represents the stiffness of the construct in the linear field of the stress-strain response. CM was selected because it is critical to the success of the implant [20], determining the response of the scaffold before permanent deformation and rupture. Consequently, the scaffold fibre material could be described as being linear elastic, through Young's modulus (E) and Poisson's ratio (ν). The mesh was described through the type of finite elements and their average dimension (SIZE); the chosen mesh was based on linear tetrahedron elements, because the architectures did not allow an efficient meshing using the hexahedron and in order to limit the computational time. Thus, only SIZE eventually varied. Therefore, in addition to geometry, the other potential inputs to the scaffold analysis were E, v and SIZE. In order to establish which of them could be neglected, so as to further simplify the analysis, it was necessary to define the sensitivity of the FEA output (CM) to them. Accordingly, a "preliminary" sensitivity FEA was conducted. FIBRE 330 µm, PORE 600 µm, STEP 90° and no OFFSET were considered as reference geometry parameters. Every other input variable differed on two levels, low and high (high = low*10). Particularly for E, 0.1 (approximately the minimum value of Young's modulus of trabecular bone) and 1 GPa; for v, 0.04 (close to the maximal compressibility) and 0.4 (close to incompressibility); for SIZE, 0.06 (a tenth of the high level) and 0.6 (default value in the FEA program). They would result in 16 combinations. Thanks to the Taguchi method it was possible to create a L4 table [19], holding only 4 principal combinations to be simulated (Table 1).

Once the sensitivity analysis had defined the most affecting parameters, the Taguchi method was used to define their principal combinations as inputs to the "final" FEA, which simulates and ranks their effects on scaffold CM.

Simulations were conducted by a FEA program (Abaqus, Simulia) as quasi-static. The geometrical inputs were described above, while the mesh and material inputs came from the sensitivity analysis. The simulated test conditions and the analysis of the

Table 1
L4 table for the sensitivity analysis.

Simulation	SIZE (mm)	E (GPa)	ν	CM (GPa)
1	0,06	0.1	0.04	0.015
2	0,06	1	0.4	0.141
3	0,6	0.1	0.4	0.018
4	0,6	1	0.04	0.123

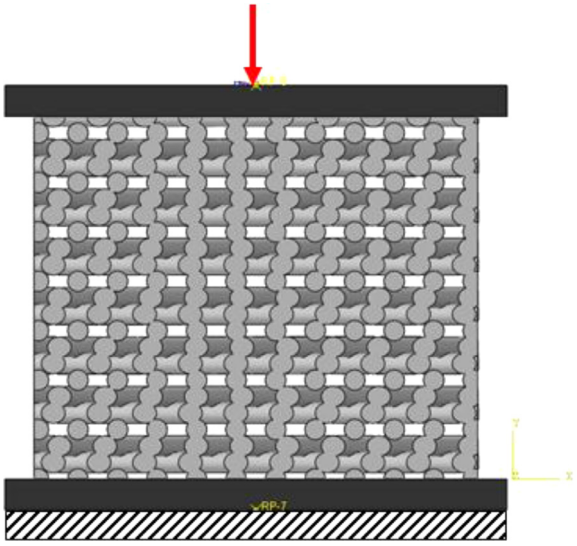

Fig. 4. Lateral view highlighting the boundary conditions on the plates (in black) compressing the scaffold (in gray) with FIBRE 330 µm, PORE 300 µm, STEP 60°, no OFFSET. The vertical (y direction) displacement of the superior plate (red arrow) is imposed, while the inferior plate is grounded. (For interpretation of the references to color in this figure legend, the reader is referred to the web version of this article.)

stress-strain curves followed the indications reported in [21]. Specifically, the plates were constrained to vertical movement only; the superior plate pressed the scaffold with a rate of 0.6 mm/s (10% of deformation per second) while the lower plate was grounded (Fig. 4). Strain was obtained as the vertical shift divided by the initial thickness of the scaffold; stress was considered as the read force divided by the initial cross-section area of the sample. CM was obtained as the gradient of the linear portion of the stress-strain curve.

Finally, FEA results were exploited to create a multiple linear regression model relating output CM (scaffold performance) to the various inputs (scaffold geometry and material), in the form of CM = f (STEP, PORE, E, ν…), thus permitting the pre-manufacturing control objective of this study. The following experimental phase served as a demonstrative application of the design procedure.

2.2. Experiments

Recently, the use of PCL/bioactive glass composites has been suggested [22], since the PCL is a medical degree polymer commonly used for tissue engineering [23] whereas the bioactive glass is well known for its osteoconductive properties. A composite of PCL (70% wt.) and bioactive glass (BGMIX-Mg) with innovative formulation (30% wt.) [14] was used as scaffold material. The novel bioactive glass (BGMIX-Mg) was obtained from a thoroughly tested bioactive glass (BGMIX) [41], by replacing a fixed 10 mol% of CaO with the same amount of MgO. The preparation of BGMIX-Mg by means of a classical melt-quenching route has already been reported elsewhere [14]. Briefly, the raw powder reagents (SiO_2, $Ca_3(PO_4)_2$, $CaCO_3$, Na_2CO_3, K_2CO_3, $(MgCO_3)_4$ $Mg(OH)_2$ $5H_2O$, by *Carlo Erba Reagenti*, Rodano-Milano, Italy) were melted at 1450 °C in a Pt crucible in air. The molten bioglass was rapidly quenched at room temperature water to obtain a frit, and was subsequently dried at 110 °C for 12 h. Finally, the frit was ground and sieved in order to obtain a powder with a final grain size lower than 25 µm.

In order to realize the composite material, poly(ε-caprolactone) (PCL, Mw 80,000 Aldrich) pellets were dissolved in chloroform (Sigma) with magnetic stirring at room temperature for 24 h. BGMIX-Mg microparticles were added to the solution during stirring, in a weight ratio of 70/30 wt.%. An ultrasonic bath (Julabo) was employed to optimize particle dispersion in the polymer solution. Excess ethanol was then added to the solution in order to obtain the precipitation of a homogeneous PCL/ BGMIX-Mg paste, and the solvent was properly removed. After drying, the obtained composites were pelletized and the pellets loaded into the tank of an auger-screw based printhead of the 3D Discovery® (RegenHU, Switzerland) bioprinting platform. In order to obtain a homogeneous melt, the pellets were kept at a temperature of 105 °C and a pressure of 3 Bar for 30 min before performing the printing process. Thereafter, the printing was performed by setting the barrel temperature to 105 °C, the pressure to 3 Bar, the screw rotation speed to 15 rpm and the printing speed to 2 mm/s. A 330 µm (FIBRE) metallic needle was used. Cylindric scaffolds ($\Phi = 10$ mm, $h_0 = 6$ mm) were designed by means of the BioCAD® software (RegenHU) by setting an interfilament distance of 930 µm (corresponding to a PORE of 600 µm) and a 0/90° deposition pattern with NO OFFSET. A layer height of 250 µm was chosen in order to optimize adhesion between adjacent layers. 5 PCL/ BGMIX-Mg 70/30 wt% scaffolds were fabricated.

Nanoindentation is useful to characterize the material at a scale proper to scaffold fibre dimension [10]. It was adopted here specifically to reveal fibre E (CM = f(E, …)). Nanoindentation tests were performed with an instrumented indenter equipped with a diamond Berkovich tip (Nanoindentation Tester NHT^2, CSM Instruments - Anton Paar S.r.l., Peseux, Switzerland); indentation hardness (H_{IT}) and elastic modulus (E_{IT}) of the scaffold fibre material were obtained according to the Oliver-Pharr method [24] considering ν equal to 0.3. Indentations at room temperature were performed perpendicular to the axis of the fibre scaffold, by adopting the following procedure: loading to maximum load in 10 s, a holding time of 60 s and unloading in 10 s. The maximum load was set in order to obtain an indentation area large enough compared to grain size (<25 µm) in order to provide information about the mechanical properties of the fibre composite material (and not of individual bioactive glass grains), but small enough to avoid the influence of both the free surface and the substrate [39]. Six indentations for each of the five analyzed scaffolds –printed in the composition of 70/30 wt.% PCL/bioactive glass - were performed in order to obtain reliable mechanical data.

In order to validate - as input of the design model CM = f (STEP, PORE, E, ν…) - the use of E_{IT} as E, the 5 printed scaffolds were tested according to ISO 844:2007 [40]. Specifically, tests were performed in air with a standard compression machine (Instron 4465) at a constant cross-head speed of 10% h_0/min until the specimen thickness was reduced to 85% of h_0. Engineering stress-strain curves were calculated from the recorded load vs. displacement data using the initial dimensions of each sample. The compressive modulus (CM, MPa) of the structure was estimated from the linear portion of the curves. The design model was not considered valid (i.e. E tuned starting from E_{IT}) until the scaffold CM obtained by FEA fell inside the experimental range (mean ± SD).

After FEA validation, the multiple linear regression that relates material, architecture and CM - applied on the simulation output– served to properly select the best performing scaffold architectures to be printed in the 70/30 wt% PCL/bioactive glass.

Table 2
Porosity of the various CAD scaffold architectures.

FIBRE	330 µm																	
PORE	300 µm						450 µm						600 µm					
STEP	90°		60°		45°		90°		60°		45°		90°		60°		45°	
OFFSET	NO	YES	NO	YES	NO	YES	NO	YES	NO	YES	NO	YES	NO	YES	NO	YES	NO	YES
Porosity	51%	50%	51%	51%	51%	50%	59%	59%	59%	60%	60%	59%	65%	65%	65%	66%	66%	65%
FIBRE	840 µm																	
PORE	300 µm						450 µm						600 µm					
STEP	90°		60°		45°		90°		60°		45°		90°		60°		45°	
OFFSET	NO	YES	NO	YES	NO	YES	NO	YES	NO	YES	NO	YES	NO	YES	NO	YES	NO	YES
Porosity	32%	31%	31%	32%	31%	31%	39%	38%	40%	39%	40%	39%	44%	44%	44%	45%	45%	45%

Table 3
a and *c* fitting parameters of Eq. (2), which relates porosity with the ratio between pore and fibre size on the scaffold architectures. As example of the fitting application, PORE* stands for the pore size needed to obtain a porosity of 60%, once the fibre dimension (3D printer nozzle) is fixed to 330 or 840 µm.

Group of scaffolds	*a*	*c*	PORE* if FIBRE 330 µm	PORE* if FIBRE 840 µm
45°-YES	104.451	−0.835	475 µm	1210 µm
45°-NO	105.989	−0.848	452 µm	1151 µm
60°-YES	105.91	−0.838	455 µm	1159 µm
60°-NO	105.246	−0.843	462 µm	1176 µm
90°-YES	103.909	−0.856	478 µm	1218 µm
90°-NO	104.67	−0.821	475 µm	1209 µm

3. Results

3.1. Simulation

Based on evaluation of scaffold CAD porosities by Eq. (1) (Table 2), only FIBRE equal to 330 µm was taken into account and, thus, the number of geometrical combinations to be analysed was reduced from 36 to 18. Specifically, geometrical combinations were pooled by STEP-OFFSET and fitting parameters of Eq. (2), which relates porosity with PORE:FIBRE, were calculated (*a*,*c* in Table 3). As suggested by previous work [1], a minimum porosity threshold of 60% was selected; by setting the printer nozzle, i.e. FIBRE (here 330 or 840 µm), a pore threshold was obtained (PORE* in Table 3). With FIBRE equal to 840 µm, PORE* would be too large, outside the optimal range described in literature [25]. Thus, scaffolds with 840 µm FIBRE were excluded.

From the sensitivity analysis, SIZE input resulted the least relevant: it was excluded from the following analyses and fixed to the FEA program default value. In particular, "preliminary" FEA gave simulated CM reported in Table 1. For each couple of rows that presented the same parameter level, average CM was calculated. Thus, a representative CM of the high and low levels for each parameter was obtained and the effect of each one was measured as ratio between corresponding high and low CM. For a tenfold variation of the input, the ratio was 8.15 for E, only slightly higher than 1 for ν (1.16) and even closer to 1 for SIZE (1.11).

Eighteen scaffold design combinations entered the "final" FEA. The list of inputs has been completed with the relative levels of FIBRE, PORE, OFFSET and STEP as geometrical inputs, and E and ν as fibre material parameters. FIBRE was set to 330 µm. PORE, STEP, E and ν varied on three levels: 300-450-600 µm for PORE; 45°-60°-90° for STEP; 0.05 (trabecular bone lower bound in [26])-0.275 (in between value)-0.5 GPa (1 order bigger than the lower bound) for E; 0.1-0.3-0.49 for ν [27]; OFFSET varied on 2 levels and defined 2 pools of architectures to be analysed separately. For each pool–composed of 4 parameters (STEP, PORE, E, ν) varying on 3 levels–$3^4 = 81$ simulations should be carried out. Thanks to the Taguchi method, these were reduced to 9, giving the L9 tables [28] (Table 4). In terms of parameter influence on FEA CM (Fig. 5), the most promising architectures have a STEP of 90° without offset and a STEP of 60° with offset, respectively. The STEP vs. CM relation is strongly proportional between STEP 45° and 60°, while it is less defined between 60° and 90°, both without and with offset. As expected for PORE vs. CM and E vs. CM, a higher porosity corresponds to a lower scaffold stiffness, vice versa a higher fibre stiffness corresponds to a higher scaffold stiffness with a strongly linear relation (**m** closed to 1 in Fig. 5).

Geometry prevailed over material in affecting scaffold CM. In particular, ranking the parameters from most to least influential (**m** of Fig. 5 from higher to lower), PORE-STEP-E-ν was obtained

Table 4
L9 Taguchi tables for the NO OFFSET and YES OFFSET combinations of FEA simulations.

NO OFFSET					
Simulation	STEP (°)	PORE (µm)	E (GPa)	ν	CM (GPa)
1	45	300	0.05	0.1	0.010
2	45	450	0.275	0.3	0.022
3	45	600	0.5	0.49	0.028
4	60	300	0.275	0.49	0.068
5	60	450	0.5	0.1	0.077
6	60	600	0.05	0.3	0.006
7	60	300	0.5	0.3	0.119
8	90	450	0.05	0.49	0.013
9	90	600	0.275	0.1	0.03
YES OFFSET					
Simulation	STEP (°)	PORE (µm)	E (GPa)	ν	CM (GPa)
1	45	300	0.05	0.1	0.008
2	45	450	0.275	0.3	0.020
3	45	600	0.5	0.49	0.025
4	60	300	0.275	0.49	0.075
5	60	450	0.5	0.1	0.044
6	60	600	0.05	0.3	0.002
7	60	300	0.5	0.3	0.085
8	90	450	0.05	0.49	0.005
9	90	600	0.275	0.1	0.010

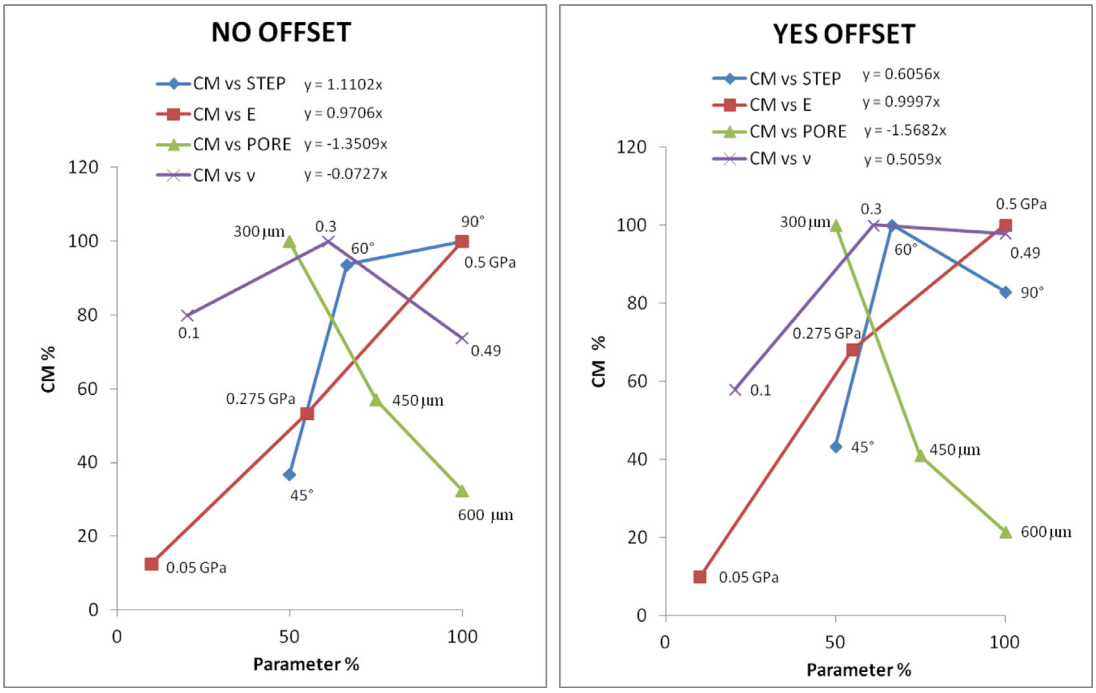

Fig. 5. Average effect on CM of the different levels of STEP, PORE, E and ν for the groups without (NO OFFSET) (left) and with offset (YES OFFSET) (right). Horizontal and vertical coordinates are expressed as% of the maximum value in the ranges, respectively, of the parameters and CM. Each marker is accompanied by its parameter level, expressed as absolute value. CM-parameter relations are fitted by a $y = mx$ function, where the gradient m becomes a sensitivity index.

Table 5
Values of the coefficients of Eq. (3) relative to the sets without (NO OFFSET) and with (YES OFFSET) offset, fitted on the rows of Table 4.

	a	b	c	d	e
NO OFFSET	0.000662	−0.000147	0.144407	−0.006630	0.026816
YES OFFSET	0.000265	−0.000146	0.102963	0.037087	0.039397

for the architectures without offset, and PORE-E-STEP-ν for the architectures with offset. However, if for STEP the range 45°–60° is considered alone, the sensitivity rank was PORE-STEP-E-ν, independently from the offset.

Once the influence of the design parameters was understood, it was possible to control it. Specifically, the following multiple linear regression was used:

$$CM = a * STEP + b * PORE + c * E + d * \nu + e \quad (3)$$

In order to obtain its specific coefficients (Table 5), the model was fitted on Table 4 combinations.

3.2. Experiments

Nanoindentation on the fibres resulted in a mean E_{IT} of 0.77 ± 0.25 GPa. To validate the FEA simulations on the chosen scaffold architecture, E_{IT} must be reduced from 0.77 to 0.23 GPa to become E in Eq. (3), resulting in a simulated CM (0.038 GPa) inside the experimental range (0.0384 ± 0.0035 GPa) of the compressive tests.

By simulating the scaffolds made by the specific PCL/bioactive glass 70/30 wt.% material (i.e. using the relative validated E) (Table 6), the STEP and PORE levels generally follow the same order of influence derived from the Taguchi combinations of geometry and generic material (Fig. 5).

By using Eq. (3) fitted on Table 4 only (coefficients of Table 5), the error of the regression model ("Reg" results in Table 6) in predicting the PCL/bioactive glass 70/30 wt.% performances ("Sim" results in Table 6) was high (see RMS in Table 6). By adding the simulations on the specific material to the regression model, updated coefficients were obtained (Table 7): the error decreased from 9.17E-5 to 4.069E-5 GPa and from 6.85E-5 to 2.49E-5 for the NO OFFSET and YES OFFSET sets, respectively.

Once the regression ability of Eq. (3) has been improved, the model can be applied to control the scaffold performances. For instance, by using the STEP 90° and imposing a porosity

Table 6
Rank of the scaffold architectures in PCL/bioactive glass 70/30 wt.% by simulation (Sim) CM, coupled with the corresponding multiple regression model (Reg) CM, for the scaffolds without offset (NO OFFSET) and with offset (YES OFFSET). RMS is the Root Mean Square of the differences between simulation and regression CM.

NO OFFSET				CM	
Rank	PORE (µm)	STEP (°)	porosity%	70/30 Sim	70/30 Reg
1	300	90	50.29	0.060	0.072
2	450	90	58.96	0.043	0.054
3	300	60	50.51	0.042	0.048
4	300	45	50.85	0.040	0.036
5	450	60	59.46	0.036	0.030
6	600	60	65.61	0.027	0.011
7	600	90	64.93	0.026	0.036
8	450	45	59.93	0.018	0.017
9	600	45	66.15	0.009	−0.001
				RMS (GPa)	9.17E-5
YES OFFSET				CM	
Rank	PORE (µm)	STEP (°)	porosity%	70/30 Sim	70/30 Reg
1	300	60	50.84	0.044	0.046
2	300	90	49.84	0.039	0.054
3	300	45	50.15	0.039	0.043
4	450	60	59.80	0.021	0.025
5	450	90	58.81	0.018	0.033
6	450	45	58.95	0.017	0.021
7	600	90	64.97	0.008	0.011
8	600	45	65.00	0.008	−0.001
9	600	60	65.95	0.008	0.003
				RMS (GPa)	6.85E-5

Table 7
Values of the coefficients of Eq. (3) relative to the sets without (NO OFFSET) and with (YES OFFSET) offset, fitted on both the rows in the general (Table 4) and 70/30 wt.% (Table 6) Taguchi tables.

	a	*b*	*c*	*d*	*e*
NO OFFSET	0.000547	−0.000118	0.145251	−0.006713	0.020298
SI OFFSET	0.000133	−0.000127	0.105332	0.036854	0.037375

threshold of 60%, a PORE of 462/455 µm is obtained for the NO OFFSET/ YES OFFSET cases, respectively. With the PCL/bioactive glass 70/30 wt.% material, applying $E = 0.23$ GPa, $\nu = 0.3$ and the specific coefficients to Eq. (3), CM of 0.046 (NO OFFSET) and 0.027 GPa (YES OFFSET) are obtained, both lower than the trabecular bone threshold (0.05 GPa in [26]). Conversely, if the CM threshold is to be reached, with STEP 90° and PCL/ bioactive glass 70/30 wt.% material, PORES of 431 and 272 µm have to be imposed, corresponding to porosities of 60% and 50% for the NO OFFSET and YES OFFSET cases, respectively. Finally, it is possible to fix both porosity (60%) and CM (0.05 GPa), thus revealing the E that the fibre material should have: again with STEP 90°, it results in $E = 0.266$ GPa (NO OFFSET) and $E = 0.475$ GPa (YES OFFSET).

4. Discussion

In this paper, the influence of the design parameters on the mechanical performances of 3D printed scaffolds has been investigated through a combined CAD/Taguchi/FEA approach (Fig. 1). Accordingly, a regression model able to control scaffold mechanics in a pre-manufacturing phase has been proposed. Interestingly, it has been found that the compressive modulus (CM) of the designed scaffold, crucial for its mechanical performance, is primarily related to its geometry–specifically to the pores size (PORE) and fibre orientation in subsequent fibres planes (STEP)–and secondly to the material–i.e. to the fibre elastic modulus (E) rather than to the Poisson's ratio. By applying the proposed method to the investigated geometries and to an innovative PCL/bioactive glass material with composition 70/30 wt%, the more promising scaffolds can be selected for 3D printing and finally tested, aiming to reach an experimental CM of 0.05 GPa (threshold for trabecular bone [26]) and a porosity of 50% (threshold for bone [29]). Considering the above constraints, four different architectures emerged as optimal: two architectures without offset (with STEP 90°: PORE 300 and 450 µm) and two with offset (PORE 300 µm: STEP 60° and 90°). Architectures with an offset - basically a shift between fibres of corresponding planes - were not discarded even if weaker, because they could provide a more effective biological response [25].

Looking at the contingent relationships among the investigated scaffold parameters and the CM, a clear and proportional relation was found only between fibre stiffness and scaffold stiffness (Fig. 5). Although the relation between geometrical parameters and scaffold mechanics resulted more complex to understand, the major influence on CM pertained to geometry rather than to material.

It is well known from structural mechanics that architecture has a prominent role in determining the structure's performances. Therefore, slight variations in the geometrical parameters can affect scaffold porosity and, thus, its mechanical response [30]. In this work, the effect of architecture variations on the CM of the construct could be explained by their potential influence on the "pillars", which determine the vertical stiffness of the scaffold (Fig. 2a,b).

Generally, the presence and size of voids strongly decrease structure strength [31]. This study once again confirmed that pore size, and thus porosity, is predominant in affecting scaffold mechanics since, in this specific context, it decreases the spatial frequency of the vertical pillars.

When an offset between corresponding layers of fibres is introduced, the vertical pillars lose their straight orientation in favour of a "zig–zag" one (orange lines in Fig. 2a, b). This definitely decreases the scaffold resistance to compressive stresses.

Finally, the influence of fibres orientation on compressive performances of the scaffold appeared strong, as reported by Ostrowska et al. [5].

The number of the analysed combinations of scaffold parameters (Table 4) was the minimum required to reveal their principal effects on the mechanics of the construct. It derived from considering the parameters independently from each other. Eventual "cross-talking" effects between them were neglected *a priori*, and this may represent a limitation of the study. In fact, based on the restricted number of combinations evaluated, only the simplest regression model, i.e. the linear one, could be used to relate design input parameters with scaffold performances, although some parameters showed a nonlinear effect (Fig. 5). In light of this, the implemented regression model should be used to exclude the less promising material-geometry combinations rather than for a precise control of the scaffold performance. Another limitation involved the scaffold model simulated by FEA: in the model validation phase, the fibre elastic modulus, E, cannot perfectly coincide with the experimental indentation elastic modulus, E_{IT}, but it had to be tuned to take into account expected deviations of the realized scaffold from the simulation CAD geometry. For instance, fibres in the scaffold model were considered fully solid, when instead internal unintended micro-pores might have been physically present [35]. An investigation of the real scaffold (for instance by SEM or μCT imaging) will better clarify the material and geometry contributions.

Concerning scaffolds aimed to regenerate bone tissue, several studies combined CAD and FEA [3,4,7–10,17,32–36], but with different modalities and purposes. Major similarities can be found in the study of Wieding at al. [37], where FEA and a DOE method (one of the techniques implemented in the Isight-Simulia software, different from the Taguchi method) were used to analyse the parameters sensitivity and to optimize the compressive modulus of the scaffold design: it found that a major influence was related to the geometrical parameters, whereas the sensitivity to the fibre elastic modulus and overall to the Poisson's ratio was minor. Nevertheless, the combined use of CAD–to analyse scaffolds porosities -, Taguchi method–to select the principal combinations of geometry and material parameters–and FEA–to simulate their influence on the scaffold performances -, in a fully pre-manufacturing design, represents an innovative procedure introduced by this study with respect to the available scientific literature.

5. Conclusions

Experimental testing provides a repeatable controlled environment for the evaluation of mechanics, but it can be cost- and time-intensive when considering multiple design iterations and large numbers of specimens [38]. In order to realize and test only the most promising scaffolds towards bone regeneration, an innovative pre-processing and pre-testing design procedure - combining in a systematic way CAD, Taguchi method and FEA - was proposed in order to analyse the effect of geometry and material on the compressive behaviour of the scaffold. Specifically, FEA was limited to the initial, linear portion of the scaffold stress-strain response, namely stiffness. Stiffness of the scaffold was influenced primarily by its geometry and secondly by its composition. Based on stiffness and porosity, four scaffold architectures were selected as optimal for the 3D printing of an innovative PCL/bioactive

glass material with composition 70/30 wt.%. Their design parameters and performances will be investigated experimentally, both mechanically and biologically. This design procedure can be adapted to any manufacturing process, scaffold material and target performance.

Acknowledgments

This study was supported by the "5 × 1000" (2016) funding, provided by the Istituto Ortopedico Rizzoli, Bologna (Italy).

Competing interests

None declared.

Ethical approval

Not required.

References

[1] Roohani-Esfahani S-I, Newman P, Zreiqat H. Design and fabrication of 3D printed scaffolds with a mechanical strength comparable to cortical bone to repair large bone defects. Sci Rep 2016;6:19468. doi:10.1038/srep19468.
[2] Dimitriou R, Jones E, McGonagle D, Giannoudis P V. Bone regeneration: current concepts and future directions. BMC Med 2011;9. doi:10.1186/1741-7015-9-66.
[3] Boccaccio A, Uva AE, Fiorentino M, Mori G, Monno G. Geometry design optimization of functionally graded scaffolds for bone tissue engineering: a mechanobiological approach. PLoS One 2016;11. doi:10.1371/journal.pone.0146935.
[4] Sahai N, Tewari RP. C Haracterization O F E Ffective M Echanical S Trength O F C Hitosan P Orous T Issue S Caffolds U Sing 2015;2:21–8.
[5] Ostrowska B, Di Luca A, Moroni L, Swieszkowski W. Influence of internal pore architecture on biological and mechanical properties of three-dimensional fiber deposited scaffolds for bone regeneration. J Biomed Mater Res Part A 2016;104:991–1001. doi:10.1002/jbm.a.35637.
[6] Wieding J, Jonitz A, Bader R. The effect of structural design on mechanical properties and cellular response of additive manufactured titanium scaffolds. Materials (Basel) 2012;5:1336–47. doi:10.3390/ma5081336.
[7] Chuan YL, Hoque ME, Pashby I. Prediction of patient-specific tissue engineering scaffolds for optimal design. Int J Model Optim 2013;3:468–70. doi:10.7763/IJMO.2013.V3.322.
[8] Wieding J, Souffrant R, Mittelmeier W, Bader R. Finite element analysis on the biomechanical stability of open porous titanium scaffolds for large segmental bone defects under physiological load conditions. Med Eng Phys 2013;35:422–32. doi:10.1016/j.medengphy.2012.06.006.
[9] Eshraghi S, Das S. Micromechanical finite-element modeling and experimental characterization of the compressive mechanical properties of polycaprolactone-hydroxyapatite composite scaffolds prepared by selective laser sintering for bone tissue engineering. Acta Biomater 2012;8:3138–43. doi:10.1016/j.actbio.2012.04.022.
[10] Martínez-Vázquez FJ, Perera FH, Miranda P, Pajares A, Guiberteau F. Improving the compressive strength of bioceramic robocast scaffolds by polymer infiltration. Acta Biomater 2010;6:4361–8. doi:10.1016/j.actbio.2010.05.024.
[11] Phanphet S, Dechjarern S, Jomjanyong S. Above-knee prosthesis design based on fatigue life using finite element method and design of experiment. Med Eng Phy 2017;43:86–91. doi:10.1016/j.medengphy.2017.01.001.
[12] Scaffaro R, Sutera F, Lopresti F. Using Taguchi method for the optimization of processing variables to prepare porous scaffolds by combined melt mixing/particulate leaching. Mat Des 2017;131:334–42. doi:10.1016/j.matdes.2017.06.025.
[13] Pyka G, Kerckhofs G, Papantoniou I, Speirs M, Schrooten J, Wevers M. Surface roughness and morphology customization of additive manufactured open porous Ti6Al4V structures. Materials (Basel) 2013;6:4737–57. doi:10.3390/ma6104737.
[14] Bellucci D, Sola A, Salvatori R, Anesi A, Chiarini L, Cannillo V. Role of magnesium oxide and strontium oxide as modifiers in silicate-based bioactive glasses: effects on thermal behaviour, mechanical properties and in-vitro bioactivity. Mater Sci Eng C 2017;72:566–75. doi:10.1016/j.msec.2016.11.110.
[15] Poh PSP, Hutmacher DW, Holzapfel BM, Solanki AK, Stevens MM, Woodruff MA. In vitro and in vivo bone formation potential of surface calcium phosphate-coated polycaprolactone and polycaprolactone/bioactive glass composite scaffolds. Acta Biomater 2016;30:319–33. doi:10.1016/j.actbio.2015.11.012.
[16] Karageorgiou V, Kaplan D. Porosity of 3D biomaterial scaffolds and osteogenesis. Biomaterials 2005;26:5474–91. doi:10.1016/j.biomaterials.2005.02.002.
[17] Chantarapanich N, Puttawibul P, Sucharitpwatskul S, Jeamwatthanachai P, Inglam S, Sitthiseripratip K. Scaffold library for tissue engineering: a geometric evaluation. Comput Math Methods Med 2012;2012. doi:10.1155/2012/407805.
[18] Bahraminasab M, Jahan A, Sahari B, Arumugam M, Shamsborhan M, Hassan MR. Using design of experiments methods for assessing peak contact pressure to material properties of soft tissue in human knee. J Med Eng 2013;2013:1–11. doi:10.1155/2013/891759.
[19] Kacker RN, Lagergren ES, Filliben JJ. Taguchi's orthogonal arrays are classical designs of experiments. J Res Natl Inst Stand Technol 1991;96:577–91. doi:10.6028/jres.096.034.
[20] Polo-Corrales L, Latorre-Esteves M, Ramirez-Vick JE. Scaffold design for bone regeneration. J Nanosci Nanotechnol 2014;14:15–56. doi:10.1166/jnn.2014.9127.
[21] ISO 844:2007(E).
[22] Cannillo V, Chiellini F, Fabbri P, Sola A. Production of Bioglass?? 45S5–polycaprolactone composite scaffolds via salt-leaching. Compos Struct 2010;92:1823–32. doi:10.1016/j.compstruct.2010.01.017.
[23] Patrício T, Domingos M, Gloria A, Bártolo P. Characterisation of PCL and PCL/PLA scaffolds for tissue engineering. Procedia CIRP 2013;5:110–14. doi:10.1016/j.procir.2013.01.022.
[24] Pharr GM. An improved technique for determining hardness and elastic modulus using load and displacement sensing indentation experiments. J Mater Res 1992;7:1564–83. doi:10.1557/JMR.1992.1564.
[25] Lee H, Hwang H, Kim Y, Jeon H, Kim G. Physical and bioactive properties of multi-layered PCL/silica composite scaffolds for bone tissue regeneration. Chem Eng J 2014;250:399–408. doi:10.1016/j.cej.2014.04.009.
[26] Feng P, Wei P, Shuai C, Peng S. Characterization of mechanical and biological properties of 3-D scaffolds reinforced with zinc oxide for bone tissue engineering. PLoS One 2014;9. doi:10.1371/journal.pone.0087755.
[27] Mott PH, Roland CM. Limits to Poisson's ratio in isotropic materials. Phys Rev B Condens Matter Mater Phys 2009;80. doi:10.1103/PhysRevB.80.132104.
[28] Chaulia PK, Das R. Process parameter optimization for fly ash brick by Taguchi method. Mater Res 2008;11:159–64. doi:10.1590/S1516-14392008000200008.
[29] Mallick S, Tripathi S, Srivastava P. Advancement in Scaffolds for bone tissue engineering: a review. IOSR J Pharm Biol Sci 2015;10:2319–7676. doi:10.9790/3008-10143754.
[30] Brunelli M, Perrault CM, Lacroix D. Mechanical response of 3D Insert ® PCL to compression. J Mech Behav Biomed Mater 2017;65:478–89. doi:10.1016/j.jmbbm.2016.08.038.
[31] Jakubowicz J, Adamek G, Pałka K, Andrzejewski D. Micro-CT analysis and mechanical properties of Ti spherical and polyhedral void composites made with saccharose as a space holder material. Mater Charact 2015;100:13–20. doi:10.1016/j.matchar.2014.12.006.
[32] Entezari A, Roohani-Esfahani SI, Zhang Z, Zreiqat H, Dunstan CR, Li Q. Fracture behaviors of ceramic tissue scaffolds for load bearing applications. Sci Rep 2016;6. doi:10.1038/srep28816.
[33] Sanz-Herrera JA, García-Aznar JM, Doblaré M. On scaffold designing for bone regeneration: a computational multiscale approach. Acta Biomater 2009;5:219–29. doi:10.1016/j.actbio.2008.06.021.
[34] De Santis R, Russo A, Gloria A, D'Amora U, Russo T, Panseri S, et al. Towards the design of 3D fiber-deposited poly(ε-caprolactone)/iron-doped hydroxyapatite nanocomposite magnetic scaffolds for bone regeneration. J Biomed Nanotechnol 2015;11:1236–46. doi:10.1166/jbn.2015.2065.
[35] Lohfeld S, Cahill S, Doyle H, McHugh PE. Improving the finite element model accuracy of tissue engineering scaffolds produced by selective laser sintering. J Mater Sci Mater Med 2015;26:1–12. doi:10.1007/s10856-014-5376-0.
[36] Williams JM, Adewunmi A, Schek RM, Flanagan CL, Krebsbach PH, Feinberg SE, et al. Bone tissue engineering using polycaprolactone scaffolds fabricated via selective laser sintering. Biomaterials 2005;26:4817–27. doi:10.1016/j.biomaterials.2004.11.057.
[37] Wieding J, Wolf A, Bader R. Numerical optimization of open-porous bone scaffold structures to match the elastic properties of human cortical bone. J Mech Behav Biomed Mater 2014;37:56–68. doi:10.1016/j.jmbbm.2014.05.002.
[38] Ali AA, Harris MD, Shalhoub S, Maletsky LP, Rullkoetter PJ, Shelburne KB. Combined measurement and modeling of specimen-specific knee mechanics for healthy and ACL-deficient conditions. J Biomech 2017;57:117–24. doi:10.1016/j.jbiomech.2017.04.008.
[39] Martinez-Vàzquez FJ, Perera FH, Miranda P, Pajares A, Guiberteau F. Improving the compressive strength of bioceramic robocast scaffolds by polymer infiltration. Acta Biomater 2010;6(11):4361–8. doi:10.1016/j.actbio.2010.05.024.
[40] Liu M, Wu C, Jiao Y, Xiong S, Zhou C. Chitosan–halloysite nanotubes nanocomposite scaffolds for tissue engineering. J Mater Chem B 2013;1(15):1987–2108. doi:10.1039/C3TB20084A.
[41] Bellucci D, Sola A, Valeria C. Low temperature sintering of innovative bioactive glasses. J Am Ceram Soc 2012;95(4):1313–19. doi:10.1111/j.1551-2916.2012.05100.x.